LETTER

Hydrogen Production with a Protonic Ceramic Membrane Reactor on Porous Fe−Cr Alloy

Haoyu Zheng, Noriko Sata, Feng Han, Amir Masoud Dayaghi, Fumitada Iguchi, Katherine Develos-Bagarinao, Truls Norby, Marit Stange, and Rémi Costa*

Read Online

ACCESS | Metrics & More | Article Recommendations | Supporting Information

ABSTRACT: A metal supported design is desirable for ceramic electro-chemical cells because of its robustness. Yet, a strong alkaline character and a refractory nature of the electrolyte material make it challenging to densify onto a steel component. Here we show a metal supported protonic ceramic cell (MS-PCC) concept enabling ~90% ceramic material savings compared to traditional cell design. The manufacturing route combines wet ceramic processing with sintering and thin film deposition at temperatures below 1000 °C. The critical diffusive elements were sufficiently confined, and the volume variation of the different functional layers was limited to maintain the integrity of the thin film electrolyte. Applied to steam electrolysis for hydrogen production, the MS-PCC enabled a current density of about −0.84 A cm^{-2} at 600 °C at a terminal voltage of 1.3 V. This concept offers incomparable perspectives for scale-up and opens up a broad range of applications for hydrogen or Power-to-X applications.

Metal-supported protonic ceramic cells
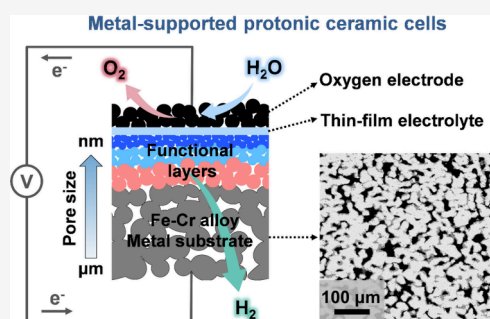
Electrolysis is a key building block for Power-to-X technologies, where X can be hydrogen, syngas, or hydrocarbons.[1] High temperature electrochemical cells operating at temperatures typically above 500 °C are especially attractive due to unrivalled energy conversion efficiency and fast kinetics.[1] Solid oxide cells (SOCs) and protonic ceramic cells (PCCs) are built upon oxygen ion conducting or proton conducting ceramic materials, respectively. Their mechanical robustness, sufficient for handling, stacking, and operating at high temperature, is conferred by increasing the thickness of one of the constitutive cell layers that can be either the electrolyte or one out of the two electrodes. This requires a substantial amount of ceramic containing critical raw materials and often enforces compromises in terms of performance.

The metal supported cell design aims at replacing thick ceramic based electrode supports by a metallic substrate, capable of withstanding both the oxidizing and reducing environment at elevated temperature and capable of supporting thin ceramic functional layers. The use of a metal substrate made of ferritic stainless-steel results in cells with a high mechanical strength and allows to reduce dramatically the amount of ceramic materials.[2−12] Nowadays, different metal supported solid oxide cells (MS-SOCs) are based on oxygen ion conducting ceramic membranes. MS-SOCs from the company CERES are currently approaching commercialization, as prototypes in the power range of 100 kW to 1 MW have recently been demonstrated for fuel cell and electrolysis application.[13,14] This technology relies on a gadolinia-doped

ceria (GDC) based electrolyte.[15] The amphoteric nature of ceria, characterized by a Smith acid−base parameter $\alpha = -2.7$, mitigates excessive reaction with volatile amphoteric or slightly acidic compounds, such as chromium oxides (Cr_2O_3), thus granting a good thermo-chemo-mechanical compatibility with the ferritic stainless-steel components.[16,17]

Yet in protonic ceramics, strong electropositive cations such as Ba confer a strong alkaline behavior ($\alpha \approx -10.8$) to perovskites from the solid solution $BaZr_{1-x-y}Ce_xY_yO_{3-\delta}$ (BZCY),[18] broadly acknowledged as the state-of-the-art PCC electrolyte material. This is a desired property to enable the incorporation of protonic defects by water uptake ($H_2O + v_O^{\bullet\bullet} + O_O^x \leftrightarrow 2OH_O^{\bullet}$ in Kröger Vink notation). However, this intrinsic property makes it highly reactive with many compounds presenting an amphoteric or acidic character, such as the volatile oxidized Cr and SiO_2 ($\alpha = 0.9$) species that could be formed and released by the stainless steel in the presence of oxygen or steam at high temperature.[3] Even though the sintering temperature can be reduced from above 1500 °C to around 1300 °C, phase decomposition and contamination of the electrolyte layer by the acidic oxides are
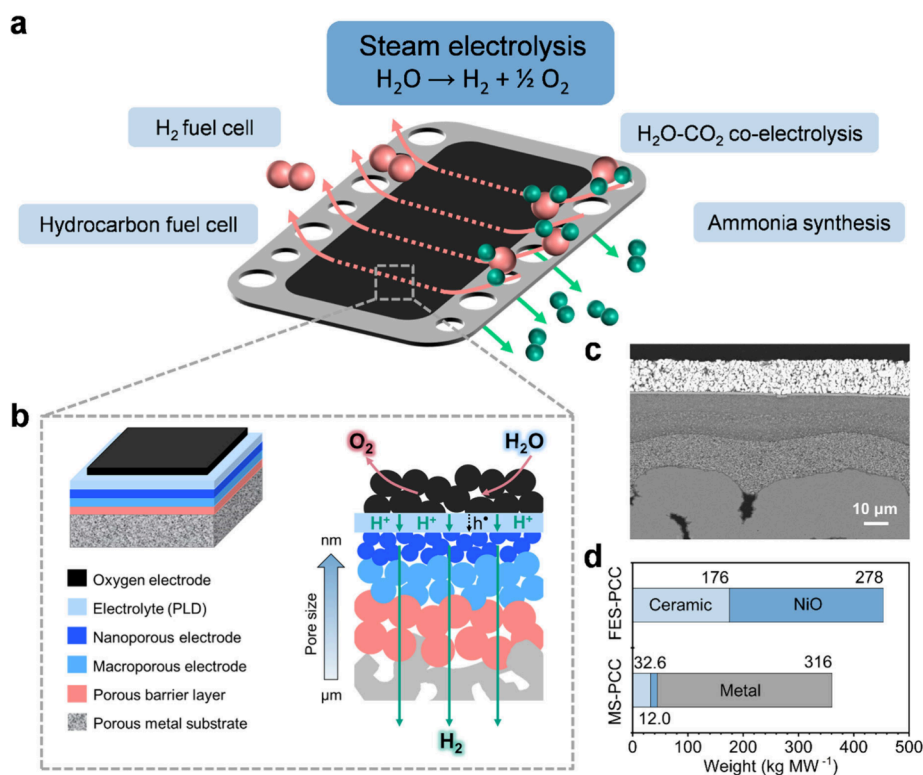
Figure 1. Concept of MS-PCC with thin-film electrolyte. (a) Schematic diagram of a MS-PCC stack cassette for Power-to-X application. (b) Illustration of the cross-sectional structure of a MS-PCC and the operating principals for steam electrolysis. (c) Cross-section SEM image of the MS-PCC with Pt oxygen electrode. (d) Estimated need of ceramic, NiO, and metal for manufacturing a MW system, comparing the MS-PCC with the fuel electrode supported protonic ceramic cell (FES-PCC) design. For the comparison, the performance values at 600 °C and 1.3 V were considered, as reported previously for FES-PCC,[24] and in this work, assuming the same faradaic efficiency. A thickness of 500 μm was set for the fuel electrode supporting layer.

commonly observed in MS-PCCs manufactured by sintering.[19] The strong alkaline character of protonic ceramics changes the paradigm of developing a metal supported cell architecture. The promising potential of PCCs has been demonstrated recently by remarkably high performances in 5 × 5 cm^2 sized cells and in reversible operation with a conventional fuel electrode supported design.[20,21] It comprises a thick (> 600 μm) fuel electrode supporting layer, which is normally a cermet of NiO mixed with the electrolyte compound. Here we demonstrate a metal-supported protonic ceramic cell (MS-PCC) concept, together with its manufacturing route (Figure S1) applied to steam electrolysis (Figure 1a). The thick cermet support is replaced by a porous metal support based on a Fe−Cr alloy, enabling an estimated ∼90% ceramic materials saving, including a 95.7% reduction in NiO, which is a strategic material for the energy transition, compared to the state-of-the-art fuel electrode supported cell architecture (Figure 1b−d).

The strategy to realize a thin and dense electrolyte is based on the fabrication of a pore graded multilayer assembly.[22,23] During manufacturing, the temperature never exceeded 1000 °C in order to prevent excessive Cr release. In this paper, we report a successful coating of dense BaZrO$_3$-based perovskite electrolyte layer on the porous metal supported substrate using pulsed laser deposition (PLD) as the key process, which is a well acknowledged thin-film fabrication technique for multi-element materials of refractory nature.

The designed cell structure contains a porous metal substrate (Figure S2), an electronic conductive diffusion barrier layer of (La$_{0.80}$Sr$_{0.20}$)$_{0.95}$MnO$_{3-\delta}$ (LSM) to avoid excessive reactivity of Cr species with the protonic ceramic material, the fuel electrode I of NiO mixed with BaZr$_{0.7}$Ce$_{0.2}$Y$_{0.1}$O$_{3-\delta}$ (NiO-BZCY721), the fuel electrode II of NiO mixed with BaZr$_{0.5}$Ce$_{0.4}$Y$_{0.1}$O$_{3-\delta}$ (NiO-BZCY541), a thin-film electrolyte of BaZr$_{0.7}$Ce$_{0.2}$Y$_{0.1}$O$_{3-\delta}$ (BZCY721), and an oxygen electrode of Pt or a composite electrode of Ba$_{0.5}$Gd$_{0.8}$La$_{0.7}$Co$_2$O$_{6-\delta}$ mixed with BaZr$_{0.5}$Ce$_{0.4}$Y$_{0.1}$O$_{3-\delta}$ (BGLC-BZCY541) as shown in Figure 1b. The different ceramic functional layers (FLs) are manufactured on top of the porous metal substrate (Figure 1c, the full cross-sectional image shown in Figure S3). A good match of the thermal expansion coefficients (TECs) between the different layers is critical to avoid cell failure. TECs of the half-cell components are listed in the Table 1.

Table 1. List of the Materials of the Half-Cell Components in This Work

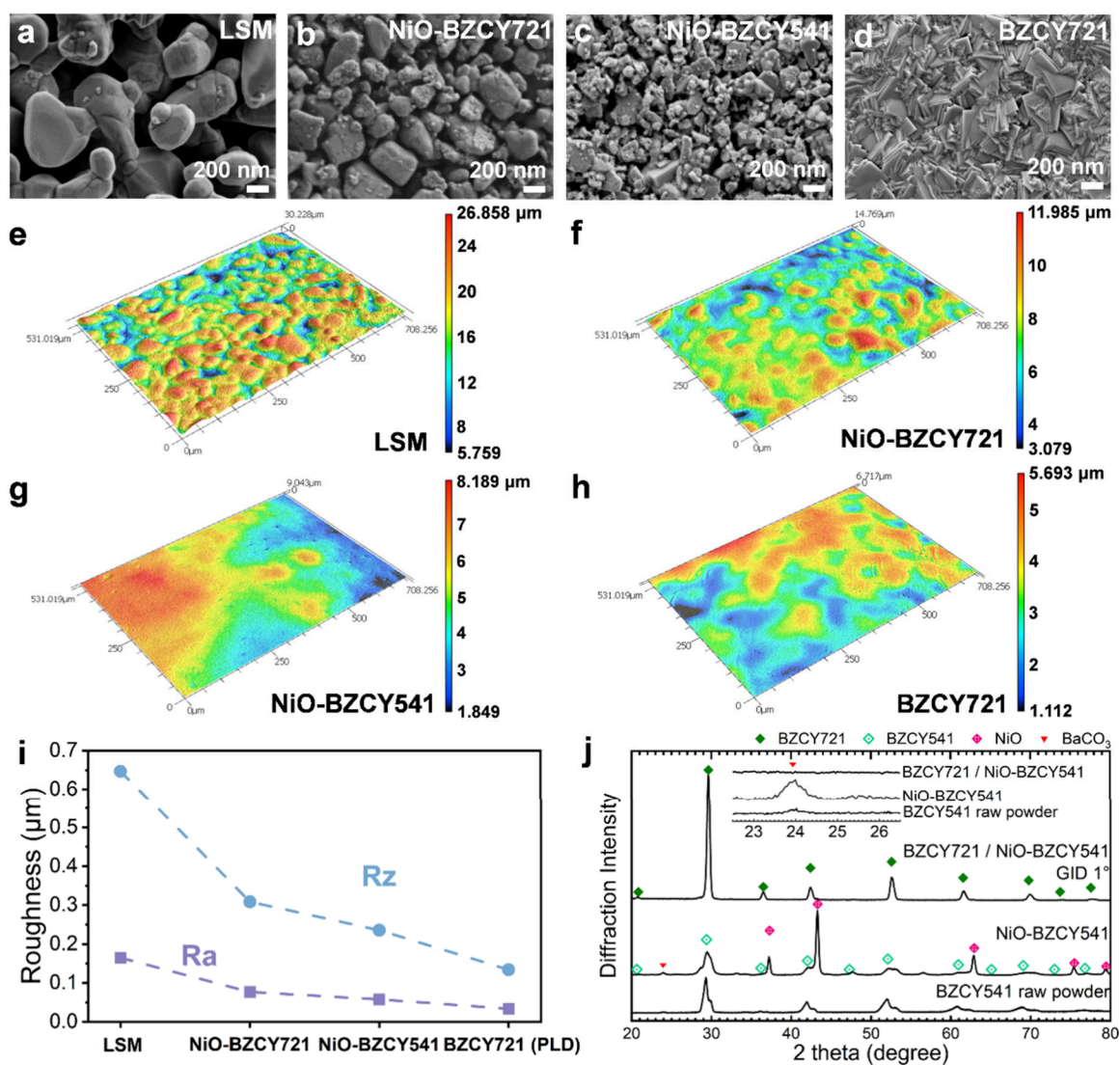| Acronym	Composition	TEC (× 10^{-6} K^{-1})	Functionality
BZCY721	BaZr$_{0.7}$Ce$_{0.2}$Y$_{0.1}$O$_{3-\delta}$	9.3[25], 10.2 @ 650−1000 °C[26]	Electrolyte
NiO-BZCY541	NiO-BaZr$_{0.5}$Ce$_{0.4}$Y$_{0.1}$O$_{3-\delta}$	11.9 @ 200−1100 °C	Fuel electrode II
NiO-BZCY721	NiO-BaZr$_{0.7}$Ce$_{0.2}$Y$_{0.1}$O$_{3-\delta}$	-	Fuel electrode I
LSM	(La$_{0.80}$Sr$_{0.20}$)$_{0.95}$MnO$_{3-\delta}$	12.4[27]	Barrier layer
ITM	Ferritic steel (26% Cr)	11.3 @ RT−900 °C	Metal support

Figure 2. Characterization of the thin-film electrolyte MS-PCC half cells. (a−d) SEM surface images of different FLs: LSM, NiO-BZCY721, NiO-BZCY541 and BZCY721, respectively. (e−h) The corresponding 3D images with topographic contrast reconstructed from the laser scanning microscope. (i) Surface roughness levels of Ra and Rz in different layers. (j) XRD diffractograms of the half cell. The diffractogram of the NiO-BZCY541 was recorded before the PLD process, and that of the BZCY721 electrolyte was recorded by a grazing incidence diffraction (GID, incident angle = 1°).

A smooth surface of the fuel electrode FL is the key to grow the thin electrolyte in good crystallinity.[28] The pore size of the metal substrate (ca. 30 μm, Figure S2) is reduced to submicron size by adding the LSM barrier layer and further reduced to ca. 200 nm by NiO-BZCY FLs (Figure 2a−d), and no obvious defects can be observed in the FLs at lower magnification in scanning electron microscope (SEM) images (Figure S4). The pore size reduction resulted in the refinement of the surface roughness (Figure 2e-h) compared to the ITM substrate (Figure S5), with an arithmetic mean roughness (Ra) of ∼0.058 μm and an average maximum peak-to-valley height of the profile (Rz) of ∼0.238 μm at the NiO-BZCY541 FL (Figure 2i). The microstructure of the MS-PCC is optimized by inserting this second fuel electrode of NiO-BZCY541 (Figure S6) as described in detail in Note S1. This high-quality surface is essential for the manufacturing of the dense electrolyte with good transport properties in order to limit the risk of pinhole formation due to the noncoverage of the underlying pores during thin film deposition. Figure S7 shows

the picture of the MS-PCC half-cell sample (5 × 5 cm^2) with the thin-film BZCY721 electrolyte on the top.

Figure 2j displays the X-ray diffractograms of MS-PCC before and after deposition of the BZCY721 electrolyte. Without the electrolyte layer, NiO, BZCY541 and a small amount of BaCO$_3$ were detected. The BaCO$_3$ originates mainly from the raw powder. The diffraction pattern of BZCY541 in the NiO-BZCY541 FL is very similar to the one of the raw powders that is characterized by a broad peak profile. This demonstrates that grain growth or phase change did not take place during the thermal treatment below 1000 °C necessary for the cell manufacturing. The electrolyte pattern was recorded by grazing incident diffraction (GID) at the incident angle of 1°, which allows to distinguish the electrolyte layer. The diffraction pattern demonstrated that the PLD coating is a well crystallized ceramic layer of the targeted BZCY721 phase.

The mechanical stability of the ceramic layers both during the manufacturing process and under operational conditions is
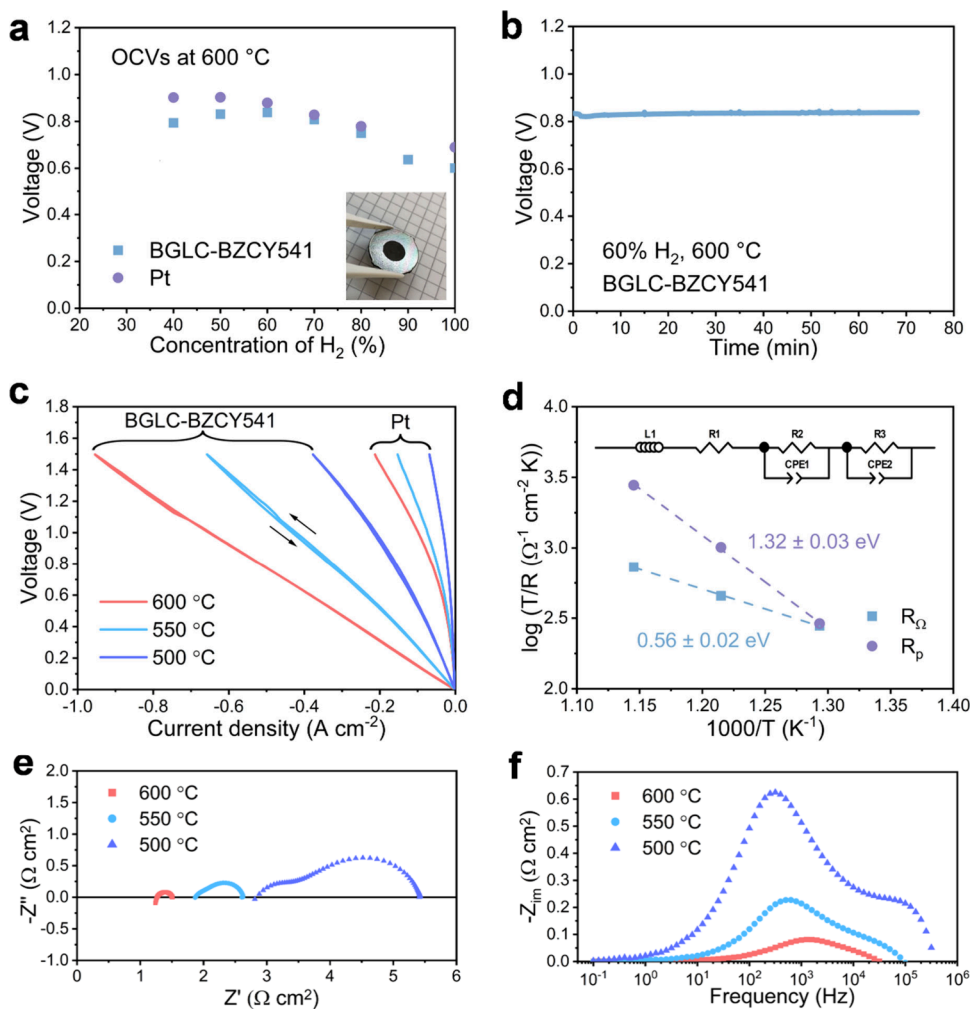
Figure 3. Electrochemical characterization of PCCs in the steam electrolysis operation. (a) OCVs of MS-PCCs with Pt or BGLC-BZCY541 oxygen electrodes obtained with different H_2 concentrations varied from 40% to 100% with N_2 balanced in the feed gas stream on the fuel electrode side, and the oxygen electrode side was supplied with 20% O_2−80% N_2; inset is the sample photo of the MS-PCC. (b) The OCV profile of the MS-PCC with 60% H_2 on the fuel electrode side. (c) Polarization curves obtained from MS-PCCs with Pt and BGLC-BZCY541 as the oxygen electrode material at temperatures between 500 °C and 600 °C. N_2 with ∼3% H_2O was supplied to the fuel electrode, and a mixture of 10% H_2O and 90% air was supplied to the oxygen electrode. Under these conditions the OCV was a few millivolts as a result of the gas conditions (no hydrogen at the fuel electrode and small pH_2O gradient); the possible gas cross over was due to the presence of pinhole defects in the electrolyte layer and the p-type charge carriers in the electrolyte, originating from the wet oxidizing gas conditions.[35] The formation of hydrogen at the fuel electrode upon polarization was evidenced with a portable hydrogen sensor at the outlet. The electrochemical impedance spectra were recorded at OCV; (d) T/R Arrhenius-type plot (analogous to σT plot) of R_Ω and R_p with BGLC-BZCY541 oxygen electrode MS-PCC, and the corresponding Nyquist impedance plot in (e), the imaginary impedance plot in (f).

crucial to achieve the desired functionality of the MS-PCC. A high stress in the electrolyte layer may cause its fracture, which would immediately degrade the cell performance. Assuming an ideal manufacturing process, the expected residual thermal stress values can be calculated with a simple model using the elastic properties[29] and thermal expansion coefficients of the materials used in the MS-PCC. By using the layer thicknesses, sintering temperatures, cermet compositions, and porosity values corresponding to the MS-PCC, the calculated stress value was −355 MPa (compressive) for a 1 μm thick BZCY721 electrolyte layer. The residual stress assessment by XRD confirmed that the electrolyte layer had compressive stress after thin film deposition (Figure S8). The stress was close to or smaller than the calculated value when the thin film electrolyte was deposited under optimal conditions (II-1 and 2 in Figure S8). When the conditions were not appropriate, the electrolyte layer could be delaminated. The samples I-1 and 2

are such examples. They presented two diffraction peaks of the PLD layer originating from the different parts grown during the deposition process due to high laser power (detail discussion in Note S2). One of these two peaks showed remarkably larger stress values which might have an origin other than purely thermal, likely in relation with the crystal growth mechanism, and that yielded the electrolyte delamination. Besides, the sufficient thermomechanical stability of the MS-PCC with a double fuel electrode layer and an optimal electrolyte was confirmed through annealing tests of the half-cells at 700 °C for 30 h (Figure S9).

The open circuit voltages (OCVs) in a H_2/O_2 concentration cell showed a double dependency on the H_2 concentration (pH_2) (Figure 3a) and on the temperature (Figure S10). Under isothermal conditions, the peak OCV was obtained for a H_2 stream diluted with N_2 with an increased viscosity—N_2 being of bigger size than the H_2 molecule—compared to a
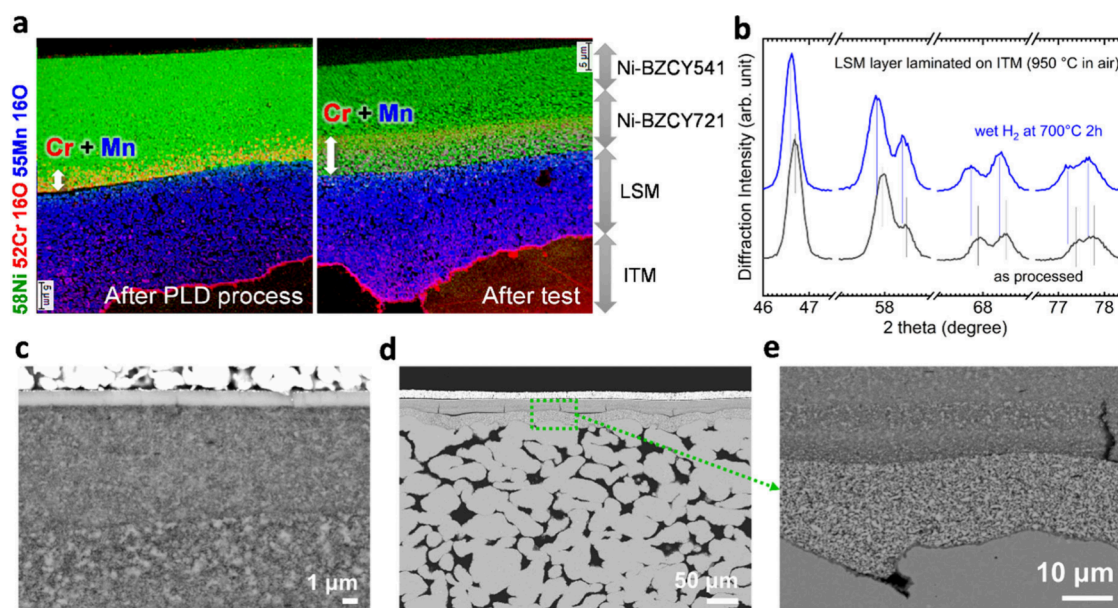
Figure 4. Degradation aspects of the MS-PCC after 200 h at elevated temperatures for electrochemical investigation. (a) Elemental mapping of the cross sections of the as-prepared (left) and tested (right) MS-PCC acquired using Nano-SIMS. For the as-prepared half-cell, it is clear that Cr and Mn diffuse into the NiO-BZCY721 layer by a few micrometers from the interface with LSM, whereas this region extends to about 10 μm after the cell test. The secondary ions are represented as follows: $^{58}Ni^-$ in green; $^{52}Cr^{16}O^-$ in red; $^{55}Mn^{16}O^-$ in blue. (b) XRD comparison of the as processed LSM layer on ITM before and after annealing in wet hydrogen. (c) SEM polished cross section with phase contrast showing the thin film electrolyte that remains crack free and well bonded with the FLs. (d) and (e) SEM polished cross section of the MS-PCC at different magnifications showing partial delamination between the FL and the LSM layer and crack formation in the FL.

pure H_2 stream. The share of hydrogen in the gas mixture corresponding to the peak of the OCV decreased upon temperature increase as the diffusivity of gases increases. This betrayed an imperfect tightness of the electrolyte or the sealing. This was confirmed by the small voltage spikes when the stability of the OCV was assessed over time (Figure 3b). The voltage spikes are likely the result of sudden variations in pH_2 and oxygen concentration (pO_2) on either side of the electrolyte due to burning. Additionally, the current leakage in the protonic ceramic electrolyte could be another reason leading to the OCV decrease.[30] Still the electrolyte is sufficiently tight to enable the cell to develop an OCVs above 0.8 V at 600 °C and to be polarized.

In PCC operated via steam electrolysis at 600 °C, the oxygen evolution reaction (OER, $2H_2O \rightarrow O_2 + 4H^+ + 4e^-$) is rate limiting. Ideally, the OER electrocatalyst should possess good proton, oxygen ion and electron transport properties. Finding a high performance and durable OER catalyst for PCC is an enduring challenge which attracts significant research focus.[31] By using Pt as an OER catalyst, a current density of ca. -170 mA cm^{-2} at 600 °C and 1.3 V (Figure 3c) could be measured in steam electrolysis operation. By using a composite oxygen electrode of $Ba_{0.5}Gd_{0.8}La_{0.7}Co_2O_{6-\delta}$ (BGLC) and BZCY541 (BGLC-BZCY541) with superior electrocatalytic and durability features,[24,32] the current density increased up to ca. -840 mA cm^{-2} at 1.3 V and 600 °C (Figure 3c). At 600 °C, the evolution of the polarization curve is almost linear over the whole range of current density, which is the reflect of a nearly constant total cell resistance (R_t). At OCV, R_t is dominated by the ohmic resistance (R_Ω), which is one order of magnitude higher than the polarization resistance (R_p) at 600 °C as determined by electrochemical impedance spectroscopy (Figure 3e and 3f). R_Ω showed an evolution in temperature between 500 °C and 600 °C that can be modeled by an

Arrhenius equation with an activation energy of about 0.56 eV (Figure 3d). Though it was difficult to deconvolute the relative contributions from the metal substrate currently, the LSM layer and the electrolyte layer that are expected to dominate R_Ω, an activation energy of 0.56 eV is consistent with protons as main charge carriers in the electrolyte material.[33] In addition, the activation energy of R_p (1.32 eV) is close to the values reported from a BGLC symmetrical cell,[34] inferring that the total MS-PCC polarization resistance is dominated by the oxygen electrode contribution. This is also consistent with the fact that the OER is rate limiting in PCC.

Beyond the electrochemical performance, the mechanical and chemical stabilities of the cells under operational conditions determine their lifetime. Figure 4a displays the elemental mapping on the cross-section of the as-prepared half-cell (left in Figure 4a) and after deposition of the oxygen electrode and electrochemical operation (right in Figure 4a) acquired with high-resolution secondary ion mass spectrometry (SIMS) imaging.

For both samples before and after test operation, Cr_2O_3 scales (represented by regions colored in red on Figure 4a) with a thickness of about 1 μm was observed on the ITM surfaces. However, the extent of Cr diffusion into the adjacent LSM layers appears more significant for the sample after operation; this can be seen as spreading of pink-colored areas adjacent to the LSM-ITM interface. The regions indicated by arrows on the Nano-SIMS images in Figure 4a also show evidence of Cr and Mn diffusion into the Ni-BZCY721 FL. The diffusion length from the LSM/Ni-BZCY721 FL interface was a few micrometres in the as-prepared cell, whereas it extended across nearly 10 μm in the tested cell in which the pores became apparently larger after the reduction. This suggests that, upon testing, Cr and Mn could be transported further into the FL due to its relatively large pore size

compared to that of the as-prepared cell. The diffusion seems to have stopped in the middle of the Ni-BZCY721 layer. At first, Cr_2O_3 vaporises and diffuses through the pores in the LSM layer during the sintering step in air at 950 °C.[16] The diffusion could be decelerated in the functional layer for several reasons, such as a decreasing pore size and reaction of the diffusing elements with the LSM to form Cr−Mn oxides. Cr and Mn could then also further diffuse during the firing of the oxygen electrode at 700 °C in oxidizing atmosphere and during the electrochemical test performed at 500−600 °C for a few hundred hours in the wet reducing conditions as applied to the fuel side in operation.[17] Though no Cr was found near the Ni-BZCY541 FL/electrolyte interface after entire electrochemical characterization, it is conceivable that Cr and Mn diffusion over a longer term would cause fatal degradation of the cells. For the long-term operation, it is therefore of high importance to minimize vaporization of Cr from the metal support during both manufacturing and operation while reducing the use of a Mn source. A dense protective coating on the metal support is, thus, highly desirable.

Cracks in the layers and delamination at the interfaces could happen when the stress is high enough to fracture or detach the layers. This can yield a significant performance loss or even operational failure of the cell. In the electrochemical ceramic cells, the most critical is the electrolyte layer, which should remain stable. SEM cross sections of tested cells (Figure 4c−e) reveal that the thin BZCY electrolyte layer exhibits no noticeable defects after operation. Observed mechanical defects are partial delamination along the LSM/Ni-BZCY721 FL interface and through-plane cracks initiated at the interface LSM/Ni-BZCY721 FL and stopped in the Ni-BZCY721 FL. From the SEM image, it is observed that cracks are located where the delamination started. Considering the small difference of the TEC values among the components, as shown in Table 1 and the fact that there is no crack in the freshly fabricated cell, the crack should have been formed during operation when exposed to the reducing atmosphere. The LSM layer calcined on ITM substrate were annealed at 700 °C for 2 h in reducing atmosphere and assessed by XRD (Figure S11). In dry hydrogen (99.999% purity), most of LSM phase was changed into $La_{1.3}Sr_{0.5}MnO_{3.95}$ and MnO, indicating Mn^{3+} reduction toward Mn^{2+}.[36] On the other hand, the LSM phase remained stable in wet hydrogen (∼3% H_2O, ∼97% H_2). Since the electrochemical operation was performed under wet atmospheres, the LSM layer might have been stable. The chemical lattice expansion in wet hydrogen was about 0.22% with respect to the as processed LSM layer (Figure 4b). The isothermal dilatometry analysis of NiO-BZCY541 cermet has determined the dimensional change in reducing condition to be at least about −0.3% (Figure S12). The dimensional change due to chemical expansion of LSM and NiO reduction in the cermet fuel electrode might be responsible for the partial delamination at the LSM/Ni-BZCY721 FL interface and for the tensile stress that resulted in crack formation in the FL.

Compared to the concepts involving manufacturing steps at high temperature, our approach of MS-PCC based on a pore graded structure processed at a temperature below 1000 °C and thin film technology is shown to be effective for application in steam electrolysis. Improvement of the Cr retention in the metal support and optimization of the different material compositions to reduce TEC mismatch between the layers and avoid excessive chemical expansion are key directions for further improving the cell performance.[37] The

implementation of other physical vapor deposition techniques to deposit the thin film electrolyte that are more industrializable than PLD could be crucial for the scale-up of the technology.

In the context of limited resources in critical and strategic raw materials for the key technologies of the energy transition, the metal supported architecture may be a key asset for the market to consider further developments. The multilayer assembly of the PCC in this architecture can also offer large selections for the counter-electrode material in replacement of the chosen oxygen electrode in this work. This opens up a broad range of applications for which PCC cells are unique. This can include electrochemical hydrogen pumping,[38] fuel cell, coelectrolysis, and diverse electrosynthesis processes including ammonia synthesis (Figure 1). In the context of the decarbonation of the energy systems, these market applications are likely to be the driver of future developments and the ramp-up of the technology.

■ ASSOCIATED CONTENT

ⓢ Supporting Information

The Supporting Information is available free of charge at https://pubs.acs.org/doi/10.1021/acsenergylett.4c01173.

> Experimental section, SEM, XRD, laser scanning confocal microscope 3D topography image of the ITM substrate, the MS-PCC sample photo, residual stress analysis of PLD coatings, and measured OCV values of the MS-PCC (Figures S1−S12); additional discussions on microstructural optimization of the MS-PCC and stress assessment of the thin-film electrolyte (Note S1−S2) (PDF)

■ AUTHOR INFORMATION

Corresponding Author

     Rémi Costa − *Institute of Engineering Thermodynamics, Electrochemical Energy Technology, German Aerospace Center (DLR), Stuttgart D-70569, Germany;* ⊙ orcid.org/0000-0002-3534-1935; Email: remi.costa@dlr.de

Authors

     Haoyu Zheng − *Institute of Engineering Thermodynamics, Electrochemical Energy Technology, German Aerospace Center (DLR), Stuttgart D-70569, Germany; Institute of Building Energetics, Thermotechnology and Energy Storage (IGTE), University of Stuttgart, Stuttgart D-70569, Germany*

     Noriko Sata − *Institute of Engineering Thermodynamics, Electrochemical Energy Technology, German Aerospace Center (DLR), Stuttgart D-70569, Germany*

     Feng Han − *Institute of Engineering Thermodynamics, Electrochemical Energy Technology, German Aerospace Center (DLR), Stuttgart D-70569, Germany;* ⊙ orcid.org/0000-0003-1904-134X

     Amir Masoud Dayaghi − *Department of Chemistry, Centre for Materials Science and Nanotechnology (SMN), University of Oslo, Oslo NO-0315, Norway*

     Fumitada Iguchi − *Department of Mechanical Engineering, College of Engineering, Nihon University, Fukushima 963-8642, Japan*

     Katherine Develos-Bagarinao − *Global Zero Emission Research Center, National Institute of Advanced Industrial*

Science and Technology, Tsukuba, Ibaraki 305-8569, Japan; ● orcid.org/0000-0001-6846-191X

Truls Norby − *Department of Chemistry, Centre for Materials Science and Nanotechnology (SMN), University of Oslo, Oslo NO-0315, Norway;* ● orcid.org/0000-0003-0909-0439

Marit Stange − *SINTEF, Oslo NO-0373, Norway*

Complete contact information is available at:
https://pubs.acs.org/10.1021/acsenergylett.4c01173

Author Contributions

H.Z. worked on the cell manufacture process, conducted microscopic structure analysis, and performed the electrochemical analysis of the cell. N.S optimized the PLD process, contributed to the structural optimization, and conducted material assessment by XRD and dilatometry. F. H. performed the early development of the cell concept and engineered the design of the metal substrate and prepared the samples for dilatometry. A.M.D. contributed to the PLD deposition, layer analysis and electrochemical test during the development phase of the thin film electrolyte. F.I. contributed to the mechanical property assessment, performed the calculation of residual stress and the XRD residual stress analysis. K.D.B. performed the investigation by Nano-SIMS. T.N. provided resources and supervision. M.S. provided resources, R.C. designed the cell and the study, provided resources and supervised the study. All coauthors discussed the results. R.C., H.Z. and N.S., prepared the first draft and all authors contributed to check-reading and revision.

Notes

The authors declare the following competing financial interest(s): The approach of manufacturing is based on a German patent application DE102016112125A1 Verfahren zur Herstellung eines Festelektrolyts, Festelektrolyt und Festoxidbrennstoffzelle since 1st of July 2016. The application is co-owned by DLR and Ceraco GmbH, and involves F.H. and R.C, and is pending (status 08.11.2023).

■ REFERENCES

(1) Hauch, A.; Kungas, R.; Blennow, P.; Hansen, A. B.; Hansen, J. B.; Mathiesen, B. V.; Mogensen, M. B. Recent advances in solid oxide cell technology for electrolysis. *Science* **2020**, *370* (6513), No. eaba6118.

(2) Bance, P.; Brandon, N. P.; Girvan, B.; Holbeche, P.; O'Dea, S.; Steele, B. C. H. Spinning-out a fuel cell company from a UK University—2 years of progress at Ceres Power. *J. Power Sources* **2004**, *131* (1−2), 86−90.

(3) Brandon, N. P.; Blake, A.; Corcoran, D.; Cumming, D.; Duckett, A.; El-Koury, K.; Haigh, D.; Kidd, C.; Leah, R.; Lewis, G.; et al. Development of Metal Supported Solid Oxide Fuel Cells for Operation at 500−600 °C. *J. Fuel Cell Sci. Technol.* **2004**, *1* (1), 61−65.

(4) Oishi, N.; Yoo, Y. Fabrication of Cerium Oxide Based SOFC Having a Porous Stainless Steel Support. *ECS Trans.* **2009**, *25* (2), 739−744.

(5) Leah, R. T.; Brandon, N. P.; Aguiar, P. Modelling of cells, stacks and systems based around metal-supported planar IT-SOFC cells with CGO electrolytes operating at 500−600 °C. *J. Power Sources* **2005**, *145* (2), 336−352.

(6) Hui, S.; Yang, D.; Wang, Z.; Yick, S.; Decès-Petit, C.; Qu, W.; Tuck, A.; Maric, R.; Ghosh, D. Metal-supported solid oxide fuel cell operated at 400−600 °C. *J. Power Sources* **2007**, *167* (2), 336−339.

(7) Xie, Y.; Neagu, R.; Hsu, C.-S.; Zhang, X.; Decès-Petit, C. Spray Pyrolysis Deposition of Electrolyte and Anode for Metal-Supported Solid Oxide Fuel Cell. *J. Electrochem. Soc.* **2008**, *155* (4), B407−B410.

(8) Hui, R.; Berghaus, J. O.; Decès-Petit, C.; Qu, W.; Yick, S.; Legoux, J.-G.; Moreau, C. High performance metal-supported solid oxide fuel cells fabricated by thermal spray. *J. Power Sources* **2009**, *191* (2), 371−376.

(9) Haydn, M.; Ortner, K.; Franco, T.; Uhlenbruck, S.; Menzler, N. H.; Stöver, D.; Bräuer, G.; Venskutonis, A.; Sigl, L. S.; Buchkremer, H.-P.; et al. Multi-layer thin-film electrolytes for metal supported solid oxide fuel cells. *J. Power Sources* **2014**, *256*, 52−60.

(10) Dayaghi, A. M.; Kim, K. J.; Kim, S.; Park, J.; Kim, S. J.; Park, B. H.; Choi, G. M. Stainless steel-supported solid oxide fuel cell with $La_{0.2}Sr_{0.8}Ti_{0.9}Ni_{0.1}O_{3-\delta}$/yttria-stabilized zirconia composite anode. *J. Power Sources* **2016**, *324*, 288−293.

(11) Udomsilp, D.; Rechberger, J.; Neubauer, R.; Bischof, C.; Thaler, F.; Schafbauer, W.; Menzler, N. H.; de Haart, L. G. J.; Nenning, A.; Opitz, A. K.; et al. Metal-Supported Solid Oxide Fuel Cells with Exceptionally High Power Density for Range Extender Systems. *Cell Rep. Phys. Sci.* **2020**, *1* (6), No. 100072.

(12) Pirou; Talic, S.; Brodersen, B.; Hauch, K.; Frandsen, A.; H; Skafte, L.; Persson, T. L., H, A.; Hogh; Henriksen, J. V. T.; H; Navasa, M.; et al. Production of a monolithic fuel cell stack with high power density. *Nat. Commun.* **2022**, *13* (1), 1263.

(13) Leah, R.; BOne, A.; Hjalmarsson, P.; Selcuk, A.; Lankin, M.; Rahman, M.; Clare, A.; Reade, G.; Felix, F.; De Vero, J.; et al. Commercialization of the Ceres Power SteelCell® Technology: Latest Update. *ECS Trans.* **2021**, *103* (1), 679−684.

(14) Leah, R.; Bone, A.; Hjalmarsson, P.; Selcuk, A.; Lankin, M.; Rahman, M.; Felix, F.; De Vero, J.; Macauley, C.; Charbonneau, C.; et al. Commercialization of Ceres SteelCell® Technology for power generation and electrolysis. *ECS Trans.* **2023**, *111* (6), 121−131.

(15) Leah, R. T.; Bone, A.; Selcuk, A.; Corcoran, D.; Lankin, M.; Dehaney-Steven, Z.; Selby, M.; Whalen, P. Development of highly robust, volume-manufacturable metal-supported SOFCs for operation below 600 °C. *ECS Trans.* **2011**, *35* (1), 351−367.

(16) Stenzel, A.; Fähsing, D.; Schütze, M.; Galetz, M. C. Volatilization kinetics of chromium oxide, manganese oxide, and manganese chromium spinel at high temperatures in environments containing water vapor. *Mater. Corros.* **2019**, *70* (8), 1426−1438.

(17) Huang, W.; Huang, T.; Song, P.; Chen, R.; Zheng, B.; Wang, C.; Li, C.; Lu, J. $CrO_2(OH)_2$ volatilization rate and oxidation behavior prediction of the NiCr coating in air-H2O environment at 650 °C. *Corros. Sci.* **2021**, *182*, No. 109303.

(18) Portier, J.; Poizot, P.; Campet, G.; Subramanian, M. A.; Tarascon, J. M. Acid−base behavior of oxides and their electronic structure. *Solid State Sci.* **2003**, *5* (5), 695−699.

(19) Wang, R.; Lau, G. Y.; Ding, D.; Zhu, T.; Tucker, M. C. Approaches for co-sintering metal-supported proton-conducting solid oxide cells with $Ba(Zr,Ce,Y,Yb)O_{3-\delta}$ electrolyte. *Int. J. Hydrog. Energy* **2019**, *44* (26), 13768−13776.

(20) An, H.; Lee, H.-W.; Kim, B.-K.; Son, J.-W.; Yoon, K. J.; Kim, H.; Shin, D.; Ji, H.-I.; Lee, J.-H. A 5 × 5 cm² protonic ceramic fuel cell with a power density of 1.3 W cm⁻² at 600 °C. *Nat. Energy* **2018**, *3* (10), 870−875.

(21) Duan, C. C.; Kee, R.; Zhu, H. Y.; Sullivan, N.; Zhu, L. Z.; Bian, L. Z.; Jennings, D.; O'Hayre, R. Highly efficient reversible protonic ceramic electrochemical cells for power generation and fuel production. *Nat. Energy* **2019**, *4* (3), 230−240.

(22) Feng, H.; Costa, R.; Robert, S. Verfahren zur Herstellung eines Festelektrolyts, Festelektrolyt und Festoxidbrennstoffzelle. German Patent DE102016112125A1,2018.

(23) Costa, R.; Han, F.; Szabo, P.; Yurkiv, V.; Semerad, R.; Cheah, S. K.; Dessemond, L. Performances and Limitations of Metal Supported Cells with Strontium Titanate based Fuel Electrode. *Fuel Cells* **2018**, *18* (3), 251−259.

(24) Zheng, H.; Riegraf, M.; Sata, N.; Costa, R. A double perovskite oxygen electrode in Zr-rich proton conducting ceramic cells for efficient electricity generation and hydrogen production. *J. Mater. Chem. A* **2023**, *11* (20), 10955−10970.

(25) Løken, A.; Ricote, S.; Wachowski, S. Thermal and Chemical Expansion in Proton Ceramic Electrolytes and Compatible Electrodes. *Crystals* **2018**, *8* (9), 365.

(26) Hudish, G.; Manerbino, A.; Coors, W. G.; Ricote, S. Chemical expansion in $BaZr_{0.9−x}Ce_xY_{0.1}O_{3−\delta}$ (x = 0 and 0.2) upon hydration determined by high-temperature X-ray diffraction. *J. Am. Ceram. Soc.* **2018**, *101* (3), 1298−1309.

(27) Tietz, F. Thermal expansion of SOFC materials. *Ionics* **1999**, *5*, 129−139.

(28) Sata, N.; Han, F.; Zheng, H.; Dayaghi, A. M.; Norby, T.; Stange, M.; Semerad, R.; Costa, R. Development of proton conducting ceramic cells in metal supported architecture. *ECS Trans.* **2021**, *103* (1), 1779−1789.

(29) Hinata, K.; Sata, N.; Costa, R.; Iguchi, F. High Temperature Elastic Modulus of Proton Conducting Ceramics Y-Doped Ba (Zr, Ce) O_3. In *Electrochemical Society Meeting Abstracts prime2020*; The Electrochemical Society, Inc,2020; pp 2617−2617.

(30) Zhu, H.; Ricote, S.; Kee, R. J. Faradaic efficiency in protonic-ceramic electrolysis cells. *J. Phys. Energy* **2022**, *4* (1), No. 014002.

(31) Papac, M.; Stevanovic, V.; Zakutayev, A.; O'Hayre, R. Triple ionic-electronic conducting oxides for next-generation electrochemical devices. *Nat. Mater.* **2021**, *20*, 301−313.

(32) Vøllestad, E.; Strandbakke, R.; Tarach, M.; Catalan-Martinez, D.; Fontaine, M. L.; Beeaff, D.; Clark, D. R.; Serra, J. M.; Norby, T. Mixed proton and electron conducting double perovskite anodes for stable and efficient tubular proton ceramic electrolysers. *Nat. Mater.* **2019**, *18* (7), 752−759.

(33) Kreuer, K. D. Proton-conducting oxides. *Annu. Rev. Mater. Res.* **2003**, *33* (1), 333−359.

(34) Strandbakke, R.; Cherepanov, V. A.; Zuev, A. Y.; Tsvetkov, D. S.; Argirusis, C.; Sourkouni, G.; Prunte, S.; Norby, T. Gd- and Pr-based double perovskite cobaltites as oxygen electrodes for proton ceramic fuel cells and electrolyser cells. *Solid State Ion.* **2015**, *278*, 120−132.

(35) Zhu, H.; Kee, R. J. Membrane polarization in mixed-conducting ceramic fuel cells and electrolyzers. *Int. J. Hydrog. Energy* **2016**, *41* (4), 2931−2943.

(36) Miyoshi, S.; Hong, J.-O.; Yashiro, K.; Kaimai, A.; Nigara, Y.; Kawamura, K.; Kawada, T.; Mizusaki, J. Lattice expansion upon reduction of perovskite-type $LaMnO_3$ with oxygen-deficit non-stoichiometry. *Solid State Ion.* **2003**, *161* (3−4), 209−217.

(37) Dayaghi, A. M.; Haugsrud, R.; Stange, M.; Larring, Y.; Strandbakke, R.; Norby, T. Increasing the thermal expansion of proton conducting Y-doped $BaZrO_3$ by Sr and Ce substitution. *Solid State Ion.* **2021**, *359*, No. 115534.

(38) Wang, Q.; Luo, T.; Tong, Y.; Dai, M.; Miao, X.-Y.; Ricote, S.; Zhan, Z.; Chen, M. Large-area protonic ceramic cells for hydrogen purification. *Sep. Purif. Technol.* **2022**, *295*, No. 121301.